Biomechanical Motion Planning for a Wearable Robotic Forearm

Vighnesh Vatsal and Guy Hoffman

Abstract—Supernumerary robotic devices in the form of wearable arms enhance a user's reachable workspace and provide them with additional capabilities. However, the user may experience considerable force and moment loads on their body due to the robot's motion. In this letter, we present a simulation and trajectory planning framework that aims to minimize the load on a user's muscles while operating a Wearable Robotic Forearm (WRF). Using a high-fidelity model of the human arm, we construct a term for biomechanical costs that is subsequently added to the overall cost function for a motion planner. For evaluation, the planner is initialized with shortest paths linearly interpolated between ten start and goal state pairs in the configuration space, as well as with paths optimized for reaction moments using a local search. We find that the biomechanical planner coupled with locally-optimized initialization reduces mean human muscle fiber forces by up to 23.47% compared to the linearly interpolated trajectories.

Index Terms—Wearable robotics, human-aware motion planning, human-centered robotics.

I. INTRODUCTION

UPERNUMERARY robotic (SR) devices are wearable augmentations, typically in the form of additional arms [1] or wrist-mounted fingers [2], that expand a user's capabilities beyond those found in nature. As opposed to prostheses and exoskeletons that aim to recreate or support existing human function [3], SR devices allow for enhanced reach, and provide the user with additional modes of interaction with the environment. However, since a user must support an SR device with their own body, one of the major challenges in their design is to reduce the ergonomic load on the human while maintaining functionality.

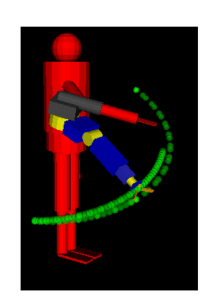
We have previously developed a Wearable Robotic Forearm (WRF) for assistance in close-range collaborative tasks using an iterative user-centered design approach [4]. The force and moment loads on a user's shoulder and elbow joints were found to be within human ergonomic ranges in scenarios involving fetching and assisted handovers [5]. This analysis, similar to [1], assumed rigid body models for both the human arm and robot, and considered the robot's effect on the user during pre-specified trajectories. In this letter, we extend the biomechanics analysis

Manuscript received December 10, 2020; accepted March 22, 2021. Date of publication April 7, 2021; date of current version April 20, 2021. This letter was recommended for publication by Associate Editor Jee-Hwan Ryu and Editor Kyle B. Reed upon evaluation of the reviewers' comments. This work was supported by the National Science Foundation under NRI Award 1734399. (Corresponding author: Vighnesh Vatsal.)

The authors are with the Sibley School of Mechanical and Aerospace Engineering, Cornell University, Ithaca, NY USA (e-mail: vv94@cornell.edu; hoffman@cornell.edu).

Digital Object Identifier 10.1109/LRA.2021.3071675





(a) WRF mounted on a user

(b) Trajectories to be optimized



(c) Upper limb musculoskeletal model [6]

Fig. 1. (a) The Wearable Robotic Forearm (WRF) is a supernumerary device for assisting the user in close-range collaborative tasks. (b) The goal of this work is to optimize the WRF's trajectories (green) to reduce loads on the user's arm muscles. (c) An OpenSim-based biomechanics model is used to determine these muscle loads, with the human arm kept static at the pose shown in (c).

by incorporating a detailed model of the human arm for determining muscle fiber forces generated due to the robot's motion. We also apply this model to develop a motion planner for finding robot trajectories that minimize human muscle loads (Fig. 1).

A. Related Work

1) Supernumerary Robotic Devices: The design of SR devices spans a wide range of sizes, functions, and mounting styles. Larger devices in the form of additional arms for tool-handling or body support are typically mounted on the user's back [1] or hips [7]. Smaller devices with mounting points on the wrists and upper forearm have been designed for grasp assistance [2] and neuro-rehabilitation [8].

Lying in between this large spectrum of sizes and functions, the WRF is mounted on a user's arm through a medical brace, with the first motor vertically aligned with their elbow (Fig. 1a). Through a series of surveys conducted earlier as part of a user-centered design process [4], we found that the most preferable function for the WRF would be as a collaborative, assistive agent in professional activities such as manufacturing, warehouse logistics management, and building construction.

2377-3766 © 2021 IEEE. Personal use is permitted, but republication/redistribution requires IEEE permission. See https://www.ieee.org/publications/rights/index.html for more information.

- 2) Biomechanics Simulation: OpenSim [9] has been widely used in the biomechanics community for dynamic simulations of human motion, with an API accessible through MATLAB [10]. Specifically for wearable robotics, combined human-robot models in OpenSim have been used for rehabilitation exoskeletons, to study their effect on the user [11], as well as to parameterically improve robot designs [12]. This letter addresses the biomechanics of interaction between the human and robot after the design phase, during usage in close-range tasks.
- 3) Manipulator Motion Planning: The motion planning problem for robotic arms has been studied extensively, with sampling-based planners being a common approach [13]. In motion planning for the WRF, a feasible trajectory may often be found by linear interpolation in the configuration space between the start and goal states (Fig. 1b). To improve upon this initial guess and minimize muscle loads, we use Stochastic Trajectory Optimization for Motion Planning (STOMP) [14], a planner that does not require gradients for its cost function. Sampling-based planners such as RRT* would require additional computation for finding a feasible initial trajectory. Aside from linearly interpolated paths, we also investigate the initialization of STOMP with a computationally inexpensive local search for generating trajectories that minimize the reaction moment loads on the human arm.

B. Contributions

The key contributions of this letter include (1) a simulation pipeline for determining the effects of a wearable robot's trajectory on the human arm, and (2) a muscle force-based approach using the above pipeline for planning ergonomically optimal robot trajectories. This pipeline is evaluated on ten start and goal state pairs for the robot. The combined OpenSim and STOMP model, on initialization with locally optimal paths, results in trajectories with up to 23.47% lower mean total muscle fiber forces compared to interpolated shortest paths in the robot's configuration space.

II. WEARABLE ROBOTIC FOREARM

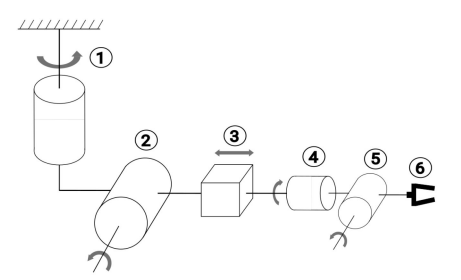
A. Design and Kinematics

The wearable robotic forearm (WRF) considered in this work is a light-weight augmentation, constructed using an arm medical brace, 3D-printed ABS and carbon-fiber reinforced plastic, and waterjet-machined aluminium structural components. It has five articulated degrees-of-freedom (DoFs) including prismatic length extension, along with a modified underactuated Yale OpenHand T42 gripper [15] as the end-effector. It is actuated using ROBOTIS Dynamixel servo motors (Fig. 2(a)). Weighing ²2 kg, it has a maximum reach of 0.63 m from the base of the first DoF. The WRF is intended to operate autonomously, with concurrent research being conducted on robot planning in collaborative tasks using human intent recognition through non-verbal communication.

Its kinematics can be described using the Denavit-Hartenberg (D-H) parameters $[\alpha, a, d, \theta]$, listed in Table I. In all trajectories considered in this work, the wrist joint and gripper are assumed



(a) WRF design with six actuators



(b) Kinematic structure of the WRF

Fig. 2. The WRF has five degrees-of-freedom (DoFs) including a prismatic joint, along with a two-fingered gripper.

TABLE I D-H PARAMETERS FOR THE WRF

Degree of Freedom	α_i	$a_i(m)$	$d_i(m)$	θ_i
(1) Horizontal panning	$\pi/2$	0	-0.08	$(-\pi, \pi)$
(2) Vertical pitching	$\pi/2$	0	0	$(0, \pi/2)$
(3) Length extension	0	0	[0.33, 0.45]	π
(4) Wrist rotation	$\pi/2$	0	0.045	$(-\pi, \pi)$
(5) Wrist pitching	$\pi/2$	0	0	$(0, \pi)$
(6) End-effector	0	0.135	0	0

to be fixed in the pose shown in Fig. 2a, with joint angles $\theta_4=0$ and $\theta_5=\pi/2$.

The start and goal states for the WRF are specified in terms of a configuration space vector $\boldsymbol{\theta} = [\theta_1, \theta_2, d_3]^T$, where θ_1 and θ_2 are the joint angles for horizontal panning (DoF-1) and vertical pitching (DoF-2) respectively, and d_3 is the length of the prismatic joint (DoF-3).

A trajectory $\Theta = [\theta_1, \theta_2, ..., \theta_N]$ is a set of N poses, going from the start state θ_1 to the goal state θ_N .

B. Dynamics Model

For a given trajectory Θ of the WRF, we can compute the force $\mathbf{F_R}$ and moment $\mathbf{M_R}$ applied at the base of the first DoF (ground link in Fig. 2b) due to the robot's motion. The WRF has five links, one between each pair of successive DoFs. As a simplifying assumption, the links are considered to be cylinders with masses, lengths, and diameters as listed in Table II.

As a further simplification, the user's arm and medical brace are considered to be a single rigid body, neglecting the contact mechanics. Since most of the structural components are mounted on the user's forearm, the corresponding reaction loads $\mathbf{F_R}$ and $\mathbf{M_R}$ are assumed to be experienced on the radius and ulna bones near the elbow joint aligned with the WRF's DoF-1 motor, as shown in Fig. 3.

TABLE II INERTIAL PARAMETERS FOR THE WRF

Link	Mass (kg)	Length (mm)	Diameter (mm)
(1)	0.470	150	55
(2)	0.425	300	68
(3)	0.457	50	35
(4)	0.248	45	25
(5)	0.350	50	35

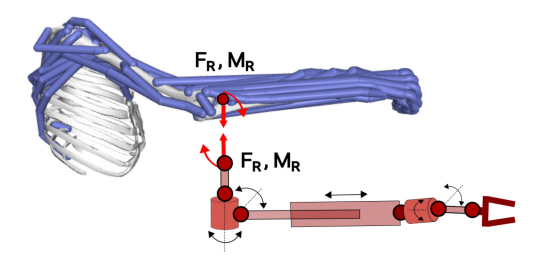


Fig. 3. The reaction force $\mathbf{F_R}$ and moment $\mathbf{M_R}$ are assumed to act on the human forearm near the elbow joint.

An iterative Newton-Euler algorithm [16] is applied to compute $\mathbf{F_R}$ and $\mathbf{M_R}$, with zero external forces and moments at the end-effector as a boundary condition. Refer to [5] for a detailed dynamics model of a previous WRF prototype, with an identical approach used in this work.

In each trajectory, the speeds of the DoFs are held constant at $\dot{\theta}_1=1.5$ rad/s, $\dot{\theta}_2=1.0$ rad/s, $\dot{d}_3=0.1$ m/s. These values were found to be the upper limits for comfortable operation of the WRF during human studies in [5]. For simplicity, the velocities are considered to start and stop instantaneously at the initial and goal states. Keeping velocities constant reduces the trajectory optimization problem to search only within the robot's configuration space. The resulting loads, $F_{\rm R}$ and $M_{\rm R}$ computed using the dynamics model, are considered to be external loads acting on the human musculoskeletal system, with the biomechanics model described in the following section used for determining muscle fiber forces.

III. HUMAN BIOMECHANICS MODEL

We aim to generate trajectories for the WRF that minimize loads on a user. To achieve this, it is first necessary to determine the effects of the WRF's motion on the user at the level of individual muscle fibers.

As described earlier, the WRF applies reaction forces $F_{\mathbf{R}}$ and moments $\mathbf{M}_{\mathbf{R}}$ on the user's forearm along each trajectory Θ . We assume that the user's intention is to hold their arm in a fixed pose while the robot moves. As a result, arm muscle fibers are activated, reacting to the external loads and holding the human's pose static during a robot trajectory.

We adapted an OpenSim-based human upper limb musculoskeletal model from [6] to estimate the active forces in these muscle fibers (Fig. 1c). It contains fifty Hill-type muscle-tendon actuators [17] with their dynamic properties as described in [18]. This model includes seven articular DoFs for the human shoulder, elbow, and wrist joints.

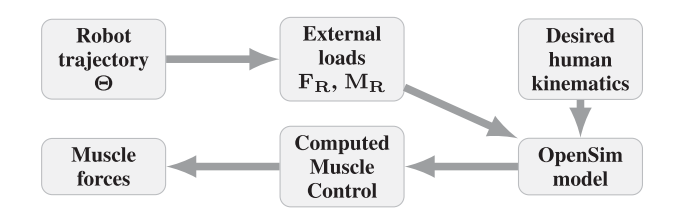


Fig. 4. Schematic of biomechanics simulation.

TABLE III DESIRED HUMAN ARM KINEMATICS

Degree of Freedom	Joint Angle (rad)	(deg)
(1) Shoulder Plane Elevation	1.0	57.3°
(2) Shoulder Elevation	1.2	68.8°
(3) Shoulder Rotation	0.3	17.2°
(4) Elbow Flexion	0.7	40.1°
(5) Elbow Pronation/Supination	0.0	0.0°

For a given robot trajectory, the computed external loads $\mathbf{F_R}$ and $\mathbf{M_R}$ are applied to the human radius and ulna bones (Fig 3). We follow a procedure similar to [12], using the MATLAB-OpenSim interface for conducting the biomechanics simulations, as shown in Fig. 4.

In the OpenSim model, external loads are considered to act on the user's joints, necessitating appropriate muscle reactions to track a desired human kinematic trajectory. The human joints of interest in this case are the three DoFs at the shoulder, and two at the elbow, while the muscles controlling wrist flexion and deviation are considered to be unaffected by the WRF's motion. For all robot trajectories in this letter, the muscle efforts aim to keep the human arm static in the pose shown in Fig. 1c, chosen to prevent human-robot collisions by design. The desired static joint angles for the shoulder and elbow are listed in Table III, with zero desired velocities and accelerations.

These kinematics are tracked using Computed Muscle Control (CMC) [19], a simulation technique that combines static optimization with feedforward control and proportional-derivative (PD) feedback control to determine the necessary muscle excitations. The forward dynamics model from [18] is used to determine the active muscle fiber lengths and active fiber forces based on these excitations.

To illustrate this simulation process, consider a trajectory $\mathbf{\Theta}^r$, going from $\theta_1 = [-1.42, 0.77, 0.43]$ to $\theta_N = [1.0, 1.57, 0.40]$ with N = 25. This trajectory represents the WRF lifting an object placed below and to the right of the user, and bringing it to their left hand, as shown in Fig. 1b. The intermediate poses θ_i , $i \in [2, N-1]$, are linearly interpolated between θ_1 and θ_N . $\mathbf{F_R}$ and $\mathbf{M_R}$ computed for $\mathbf{\Theta}^r$ using the WRF's dynamics model

The CMC simulation divides this trajectory into 20 time steps for which the kinematic errors are determined after every iteration. The PD feedback control gains for tracking each human joint are set to $K_p=400$ and $K_v=40$, in order to achieve critically-damped error dynamics [19] with $K_v=2\sqrt{K_p}$. The resulting muscle excitations are interpolated, in this case to 335 steps, and used to determine the active human muscle fiber forces $\mathbf{f}_{h,i}, i \in [1,50]$ along the trajectory.

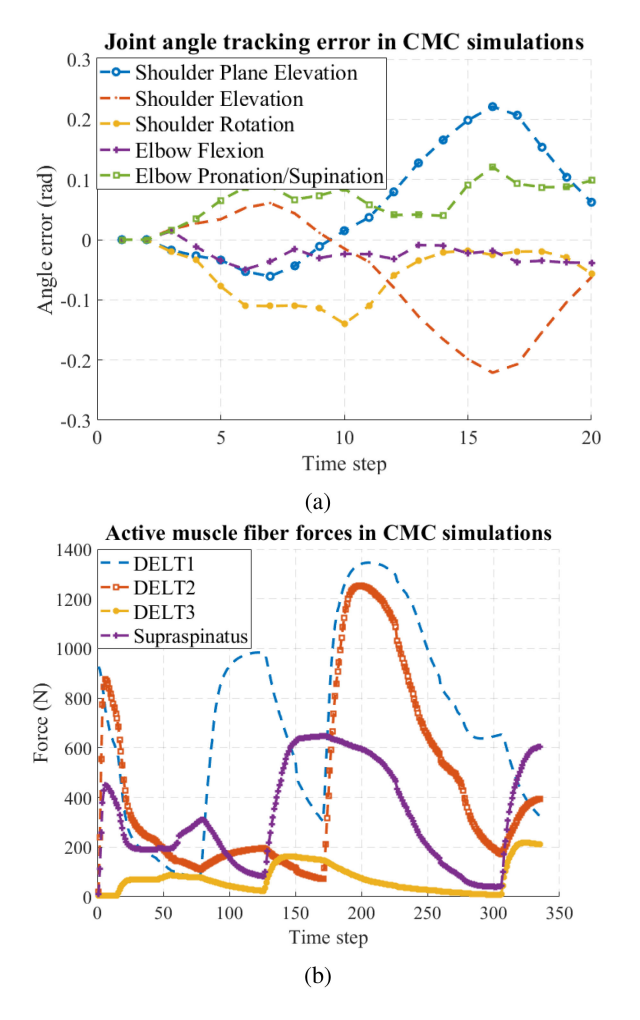


Fig. 5. Illustrative CMC results for the trajectory Θ^r : (a) tracking errors in human joint angles are below 0.25 rd, (b) active muscle forces in four fibers.

Fig. 5 illustrates the results of this CMC simulation for Θ^r . The joint angle errors for tracking the static pose are below 0.25 radians (14.3°) in the five human kinematic DoFs of interest. Fig. 5b shows the estimated active fiber forces in the first four shoulder muscles as listed in [6]: three muscles forming the deltoid group, and the supraspinatus.

We consider the first 32 muscles listed in [6], corresponding to the human shoulder and elbow joints to be relevant, and assume that the WRF's motion has no effect on the wrist and hand muscles. The fiber forces generated in these muscles form the basis of trajectory optimization and planning described in the next section.

IV. TRAJECTORY OPTIMIZATION

The planning framework uses the biomechanics model described above to generate ergonomic WRF trajectories. While the overall goal is to plan trajectories that minimize the muscle fiber forces in the user's arm, in the interest of faster convergence, the cost function for the planner also includes other factors that positively correlate with this muscle force, e.g. reaction force and moment norms, and smoothness of the trajectory. We

also describe an approach for improving the initialization of the planner.

A. STOMP With CMC

The backbone for planning WRF trajectories in this letter is STOMP, chosen since it allows for the specification of a customized state-dependent cost function without the requirement of gradients for the costs [14]. The optimization objective is formulated as follows:

$$Q(\Theta) = \mathbf{w}_{a}^{T} \Theta^{T} \mathbf{R} \Theta + \mathbf{w}_{q}^{T} \mathbf{q}(\Theta)$$
$$\Theta^{*} = \arg \min_{\Theta} Q(\Theta)$$
(1)

Starting with an initial trajectory Θ^0 , the optimal trajectory Θ^* minimizes the total cost $Q(\Theta)$ —a weighted sum of squared accelerations $\Theta^T \mathbf{R} \Theta$, and state-dependent costs $\mathbf{q}(\Theta)$. The first term contains $\mathbf{R} = \mathbf{A}^T \mathbf{A}$, derived from a second-order finite differencing matrix \mathbf{A} , and incentivizes smoothness of the resulting trajectories.

The STOMP algorithm generates K noisy trajectories around the initial guess Θ^0 , and weighs them based on the cost $Q(\Theta_K)$ to estimate a stochastic gradient update, repeating this process over successive iterations.

The state-dependent trajectory cost function contains five individual terms, $\mathbf{q}(\mathbf{\Theta}) = [q_h\,,q_f\,,q_m\,,q_{df}\,,q_{dm}]^T$, defined as follows:

1) Human Muscle Cost q_h : For each noisy trajectory Θ_K , a CMC simulation is performed as described in Section III to obtain the muscle fiber forces generated in the user's right arm due to the WRF's motion along Θ_K .

$$q_h = \sum_{j=1}^{M} F_{h,j}(\mathbf{\Theta}_{\mathbf{K}}) \tag{2}$$

The total fiber force $F_{h,j}$ for muscle j is the L_1 norm of the force vector $\mathbf{f}_{h,j}$ (Fig. 5b) interpolated for that muscle along $\mathbf{\Theta}_{K}$. q_h is computed for the first M=32 muscles in the OpenSim model, with the wrist and hand muscles excluded.

2) Reaction Load Costs q_f and q_m : The costs q_f and q_m account for the total reaction force $\mathbf{F_R}$, and reaction moment $\mathbf{M_R}$ experienced by the user. The norms of $\mathbf{F_R}$ and $\mathbf{M_R}$ are summed for each pose $\boldsymbol{\theta_i}$, $i \in [1, N]$ along a noisy trajectory $\boldsymbol{\Theta_K}$:

$$q_f = \sum_{i=1}^{N} \|\mathbf{F}_{\mathbf{R}}(\boldsymbol{\theta_i})\|$$
, $q_m = \sum_{i=1}^{N} \|\mathbf{M}_{\mathbf{R}}(\boldsymbol{\theta_i})\|$ (3)

3) Load Deviation Costs q_{df} and q_{dm} : In addition to direct costs q_f and q_m for the reaction loads, q_{df} and q_{dm} penalize positive deviations from the initial trajectory Θ^0 , and reward negative deviations. This allows for a more aggressive optimization towards a low-cost path, as shown in Fig. 12.

The deviations are computed based on the relative difference in force and moment norms at each pose between a candidate trajectory Θ_K and the initial trajectory Θ^0 . The relative difference in force, ΔF_i at step i, is defined as:

$$\Delta F_i = \frac{\|\mathbf{F}_{\mathbf{R}}(\boldsymbol{\theta}_i)\| - \|\mathbf{F}_{\mathbf{R}}(\boldsymbol{\theta}_i^0)\|}{\|\mathbf{F}_{\mathbf{R}}(\boldsymbol{\theta}_i^0)\|}$$
(4)

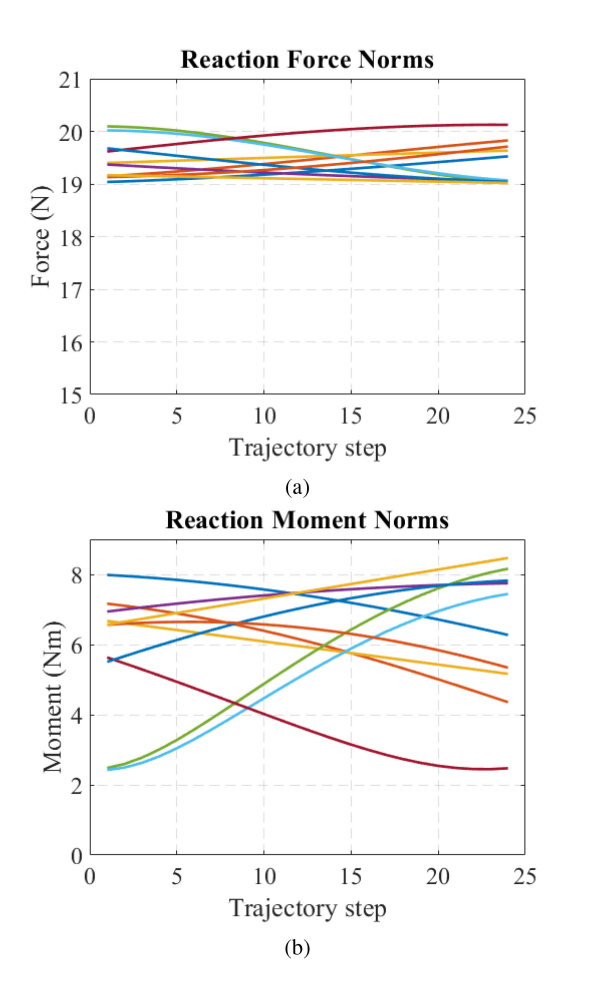


Fig. 6. (a) Reaction force norms $\|\mathbf{F}_{\mathbf{R}}\|$, vary much less than (b) moment norms $\|\mathbf{M}_{\mathbf{R}}\|$, along the linearly interpolated trajectories between the ten start and goal state pairs.

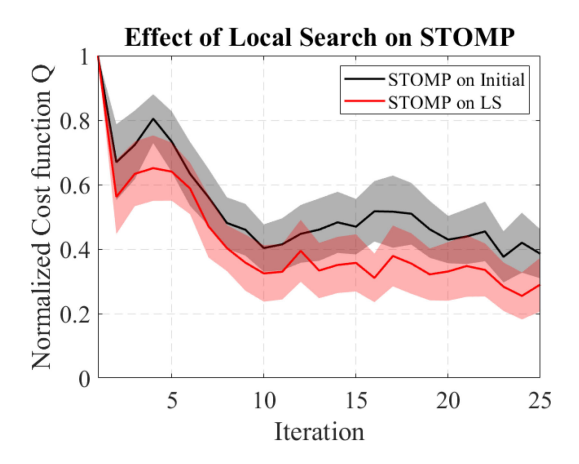


Fig. 7. On average, local search (red) leads to an improvement in the STOMP cost function over linearly interpolated initial trajectories (black).

Depending on the sign of ΔF_i , a corresponding deviation metric $d_{f,i}$ can be obtained as follows:

$$d_{f,i} = \begin{cases} e^{(\lambda_1 \Delta F_i)} - 1, & \Delta F_i \le 0\\ e^{(\lambda_2 \Delta F_i)} - 1, & \Delta F_i > 0 \end{cases}$$
 (5)

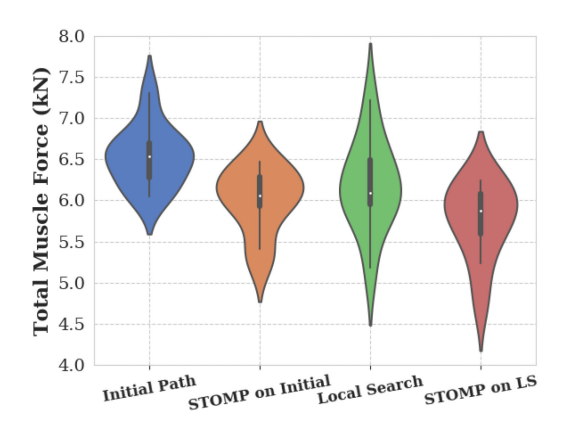


Fig. 8. Violin plots (box plots with kernel density estimates) of mean total muscle fiber force data for all ten trajectories.

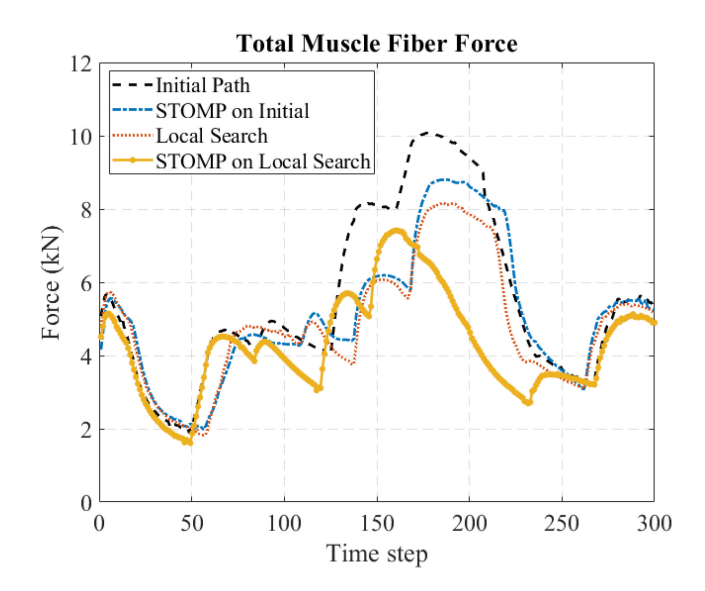


Fig. 9. Comparison of total muscle fiber force q_h for trajectory R-1 from Table V.

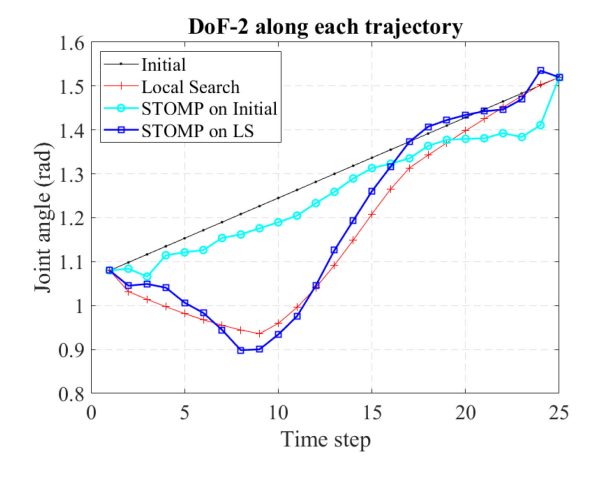


Fig. 10. Vertical pitching angle (DoF-2) for trajectories corresponding to R-1 from Table V.

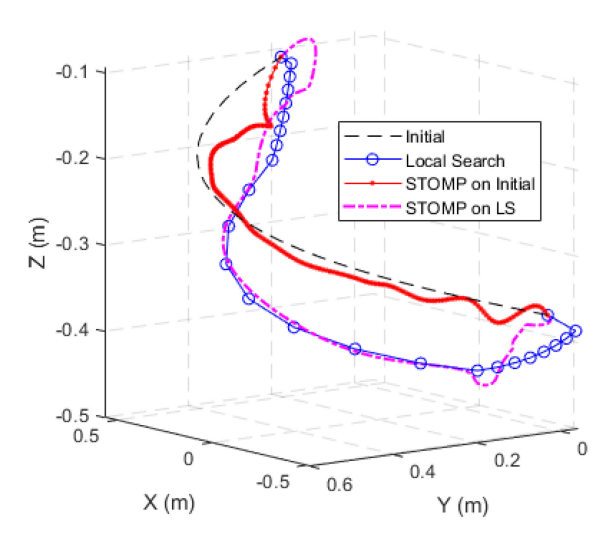


Fig. 11. End-effector positions in 3D for trajectories corresponding to R-1 from Table V.

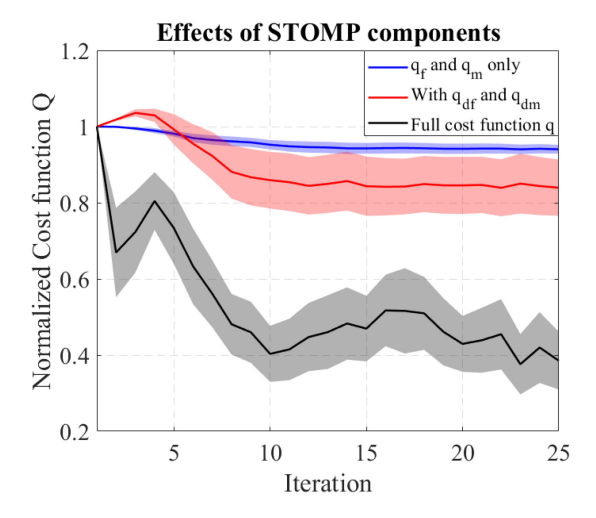


Fig. 12. Adding each component to the STOMP cost function results in an improvement in performance. (Solid lines: mean normalized costs; shaded regions: standard errors).

where $\lambda_1 < \lambda_2$, resulting in a higher positive penalty for large increases in the reaction force norm. A similar procedure is applied to compute the deviation metric $d_{m,i}$ for the reaction moment norm:

$$\Delta M_i = \frac{\|\mathbf{M}_{\mathbf{R}}(\boldsymbol{\theta}_i)\| - \|\mathbf{M}_{\mathbf{R}}(\boldsymbol{\theta}_i^0)\|}{\|\mathbf{M}_{\mathbf{R}}(\boldsymbol{\theta}_i^0)\|}$$
(6)

$$d_{m,i} = \begin{cases} e^{(\lambda_1 \Delta M_i)} - 1, & \Delta M_i \le 0 \\ e^{(\lambda_2 \Delta M_i)} - 1, & \Delta M_i > 0 \end{cases}$$
 (7)

Using these metrics, the total deviation costs for a trajectory are defined as follows:

$$q_{df} = \sum_{i=1}^{N} d_{f,i} , q_{dm} = \sum_{i=1}^{N} d_{m,i}$$
 (8)

There is a trade-off between the range of exploration for the noisy trajectories and the rate of convergence. We set the number of noisy trajectories sampled in each iteration, K=8,

TABLE IV PERCENTAGE REDUCTIONS IN MEAN q_h FOR ALL METHODS COMPARED TO LINEARLY INTERPOLATED INITIAL TRAJECTORIES

Trajectory	Percentage reduction for method: (%)			
Trajectory	STOMP on Initial	Local Search	STOMP on LS	
(1) SH-1	11.37	2.95	14.26	
(2) SH-2	13.66	1.14	14.41	
(3) A2PH	1.35	0.31	1.68	
(4) R-1	9.36	7.74	11.03	
(5) R-2	7.90	6.29	9.15	
(6) R-3	7.08	5.19	8.90	
(7) R-4	1.06	9.22	10.97	
(8) R-5	3.05	0.63	6.60	
(9) R-6	15.44	16.88	23.47	
(10) R-7	10.28	3.64	18.08	

and find that STOMP converges at around 25 iterations for each of the ten pairs of start and goal states considered in this work. However, even with a relatively small number of iterations, the task of finding a trajectory with low muscle fiber forces is computationally expensive, owing to the CMC simulations which require over an hour per iteration on a desktop workstation (Intel Core i7-9700, 32 GB RAM).

B. Local Search for Initialization

Within the constraint of computational costs for CMC, we improve the convergence of STOMP by generating better trajectories for its initialization while keeping the number of iterations fixed at 25.

Starting with the linearly interpolated shortest paths in configuration space between the start and goal states, we find a trajectory that minimizes the norm of the reaction moment $\mathbf{M_R}$. This strategy emerged from an observation of the trends for reaction forces and moments, $\mathbf{F_R}$ and $\mathbf{M_R}$. Across the linearly interpolated trajectories between all ten pairs of start and goal states considered in this letter, relatively little variation was seen in $\|\mathbf{F_R}\|$ (between ~19 and ~21 N) compared to the variation in $\|\mathbf{M_R}\|$ (between ~2 and ~9 Nm), as shown in Fig. 6.

The moment-minimizing trajectory Θ_M^* , consisting of poses θ_i^* , is determined by local minimization in a greedy manner along successive steps from the start state to the goal state:

$$\boldsymbol{\theta_i^*} = \arg\min_{\boldsymbol{\theta_i}} \|\mathbf{M_R}(\boldsymbol{\theta_i})\|^2$$
 (9)

An interior-point algorithm [20] is used to compute θ_i^* , with the gradient and Hessian of $\|\mathbf{M_R}\|$ with respect to $\boldsymbol{\theta}$ computed symbolically. The lower and upper bounds for feasible configurations are determined by the speeds of each DoF, $\dot{\theta}_1$, $\dot{\theta}_2$, and \dot{d}_3 , considered to be constant as described in the dynamics model. For instance, the horizontal panning joint angle θ_1 is bounded by $[\theta_1 - \dot{\theta}_1 \Delta t, \theta_1 + \dot{\theta}_1 \Delta t]$, where Δt is the maximum trajectory time ΔT (taken to be 3 s) divided by the number of steps N. The algorithm is initialized with the trajectory $\boldsymbol{\Theta}^0$, consisting of linearly interpolated poses between $\boldsymbol{\theta}_1^0$ and $\boldsymbol{\theta}_N^0$.

Although the STOMP cost function $Q(\Theta)$ already contains a term for $\|\mathbf{M}_{\mathbf{R}}\|$, explicitly optimizing for it in the local search before starting the STOMP iterations led to an improvement over initial trajectories obtained through linear interpolation.

Trajectory	Start State $ heta_1$	Goal State $ heta_N$	Mean Total Muscle Fiber Force (N)			
Trajectory			Initial	STOMP on	Local	STOMP on
			Path	Initial Path	Search	Local Search
(1) Reaching for object (SH-1)	[0.00, 1.57, 0.33]	[-1.42, 0.77, 0.43]	6105.84	5411.82	5925.77	5235.18
(2) Handing over object (SH-2)	[-1.42, 0.77, 0.43]	[0.00, 1.57, 0.33]	7298.53	6301.19	7215.32	6246.42
(3) Assisted two-person handover (A2PH)	[-1.33, 0.89, 0.41]	[2.41, 0.03, 0.45]	6052.42	5970.94	6033.73	5950.68
(4) Random-1 (R-1)	[3.08, 1.08, 0.43]	[0.32, 1.52, 0.40]	6425.37	6357.45	5832.79	5720.25
(5) Random-2 (R-2)	[1.00, 1.57, 0.41]	[-3.00, 0.95, 0.43]	6521.30	5910.62	6016.74	5802.18
(6) Random-3 (R-3)	[1.85, 1.43, 0.38]	[-2.62, 0.62, 0.41]	6554.13	6036.47	6141.92	5954.56
(7) Random-4 (R-4)	[2.34, 1.08, 0.42]	[-1.61, 0.82, 0.39]	6721.73	6245.51	6372.70	6123.26
(8) Random-5 (R-5)	[2.55, 0.08, 0.44]	[-1.35, 1.55, 0.42]	6626.21	6464.93	6668.06	6227.89
(9) Random-6 (R-6)	[1.23, 0.06, 0.39]	[-1.06, 1.56, 0.38]	6227.89	5266.09	5176.58	4765.93
(10) Random-7 (R-7)	[1.98, 1.42, 0.34]	[-2.15, 1.52, 0.44]	6770.48	6074.39	6524.06	5546.47

 $\label{total muscle fiber forces for Ten Start and Goal State Pairs} Table V$ Mean Total Muscle Fiber Forces for Ten Start and Goal State Pairs

Fig. 7 shows the means and standard errors for the cost functions, normalized by the cost of the first iteration, for each of the ten start and goal state pairs, resulting from STOMP performed on the linearly interpolated configuration space trajectories, and on the results from the local search. As discussed in the next section, this approach consistently generated trajectories with reduced muscle fiber forces compared to the other methods.

V. RESULTS

In this section, we compare WRF trajectories computed using all the methods described above, for ten start and goal state pairs.

The biomechanical STOMP-based optimization is performed twice for each pair, first using an initial guess for the trajectory, and then using the result from the local search. The initial guess for a valid trajectory is the linear interpolation between the start and goal states in configuration space. The local search-based approach finds a trajectory around this initial guess that minimizes the reaction moment norm $\|\mathbf{M}_{\mathbf{R}}\|$.

The results for mean total muscle fiber forces from CMC simulations on the outputs from each of these four approaches are listed in Table V. Trajectories (1) and (2) correspond to two stages of the task shown in Fig. 1 b: a self-handover (SH-1 & 2), and (3) represents an assisted two-person handover (A2PH) as described in [5]. All others are randomly generated in the WRF's configuration space (R-1 to R-7) with a path length of at least 0.8 m.

As listed in Table V, STOMP performed on the local search output consistently results in WRF trajectories with lower mean total muscle fiber force loads on the human arm compared to the other approaches. The degree of improvement for each of the methods compared to the linearly interpolated trajectories varies with the start and goal state pairs (Table IV). The local search outputs improve upon the initial linearly interpolated paths, but do not consistently outperform STOMP on the initial trajectory. The local search tends to outperform STOMP on the linear interpolation in cases where the noisy trajectories generated by STOMP are unable to explore the configuration space widely enough. As shown in Fig. 8, STOMP with either initialization has a lower variance than the local search output alone, and skews towards lower mean total muscle fiber forces. The median improvements for STOMP on local search, compared to the initial interpolated paths is by 11.00%, compared to STOMP on the initial by 2.61%, and compared to local search alone by 5.26%. Among all trajectories, the maximum improvement over the initial trajectory is for STOMP on local search (23.47% for R-6).

Looking at a specific start and goal state pair, we illustrate the effects of each of the trajectory generation approaches. Consider the start state $\theta_1 = [3.08, 1.08, 0.43]$ and goal state $\theta_N = [0.32, 1.52, 0.40]$, with N = 25 (Trajectory (4) R-1, from Table V). The STOMP cost component q_h , the total muscle fiber force along a trajectory, is shown in Fig. 9 for all four approaches, interpolated to 300 steps. The STOMP optimal trajectory initialized on the linearly interpolated configuration space results in a lower mean total muscle load, but does not explore far enough to reduce it significantly (from ~6.42 kN to ~6.36 kN). The local search is able to quickly find a trajectory that pitches lower in the Z-direction than the initial (Fig. 10), reducing the WRF's moment arm about the user's elbow. The enhancement in extent of exploration due to local search can also be seen in Fig. 11. For this start and goal state pair, the local search even outperforms STOMP on the initial guess, with a result of ~5.83 kN. Further STOMP iterations performed on the local search result reduce the load to ~5.72 kN. Although the optimal result in this case may take longer to execute on the WRF, relative trajectory times are not considered to be a factor at this stage, with the upper limit on completion being 3 seconds. Within this constraint, biomechanically superior trajectories are preferred over quicker ones.

A. STOMP Cost Function Ablation

We performed an ablation study to determine the effect that each component of the state-dependent cost $\mathbf{q}(\Theta)$ has on the overall performance of STOMP. For all ten start and goal state pairs, the total cost $Q(\Theta)$ was computed for STOMP performed using subsets of the terms in $\mathbf{q}(\Theta)$, initialized on linearly interpolated trajectories Θ^0 for 25 iterations. To compare the effects of the components, the total costs were normalized, dividing them by $Q(\Theta^0)$ to provide the relative improvements in performance shown in Fig. 12.

At first, only the effects of the direct reaction load costs, q_f and q_m , were considered. This resulted in a small relative improvement over $Q(\Theta^0)$, with a mean reduction of ~6%. Adding the load deviation costs q_{df} and q_{dm} improved this performance to a ~16% mean reduction. Finally, adding the cost term q_h from the muscle fiber forces computed through CMC resulted in a ~61% mean relative reduction over $Q(\Theta^0)$.

Including all of the components in the cost function helped generate trajectories with reduced biomechanical loads, even with a relatively small number of iterations.

VI. CONCLUSION

This letter presents a muscle simulation model for determining the load of a supernumerary wearable robot's motion on the user, and then proposes a STOMP-based optimization planner to find trajectories that minimize human muscle loads. We compare different initialization paths for the planner, including linear interpolation and locally-optimal paths, and consistently find that our method generates trajectories that reduce human muscle loads.

While these are promising results, our analysis relied on several assumptions: the speeds of the motors were held constant; the human pose was kept static as the robot moved; and it was assumed that there would be no collisions between the human and robot at any stage. These assumptions simplified the dynamics analysis, and reduced the computational cost of the simulations. In reality, we can expect the human to move in response to the robot's movement, sometimes aiding and sometimes hindering the robot's plan. While human movement would not change the mathematics of our model, and could theoretically be included into the CMC simulation, it would significantly increase computational cost.

As is, the STOMP and CMC simulations were far from realtime, requiring several hours to compute on typical hardware associated with robotic arms. Approximate methods could aid in deploying our method on a real-time physical system. These could include training a neural network regression model on a large dataset of simulated muscle forces generated in the human arm by external loading due to robot motion. Other approaches could be to reduce the size of the biomechanics model by identifying synergies between muscle groups, and to reduce the scope of the optimization problem through methods such as principal component extraction [21].

Another limitation of this work is that numerical simulations do not capture all the details involved in the user experience of wearing an SR device, which includes factors such as jerks on the wearer's body from the motors, and shear on the human skin at the interface with the mounting platform. Experimental human factors studies with our approach are needed for determining real ergonomic improvement.

Despite these limitations, the framework presented in this letter can assist in the design, biomechanical analysis, and motion planning for SR devices, allowing them to be effective agents in human-robot collaboration tasks.

REFERENCES

 C. Davenport, F. Parietti, and H. H. Asada, "Design and biomechanical analysis of supernumerary robotic limbs," in *Proc. ASME Dyn. Syst.* Control Conf., 2012, pp. 787–793.

- [2] F. Wu and H. Asada, "Supernumerary robotic fingers: An alternative upperlimb prosthesis," in *Proc. ASME Dyn. Syst. Control Conf.*, V002T16A009, 2014
- [3] M. Bergamasco and H. Herr, "Human-robot augmentation," in Springer Handbook Robot., Springer, 2016, pp. 1875–1906.
- [4] V. Vatsal and G. Hoffman, "Wearing your arm on your sleeve: Studying usage contexts for a wearable robotic forearm," in *Proc. 26th IEEE Int.* Symp. Robot Hum. Interactive Commun., 2017, pp. 974–980.
- [5] V. Vatsal and G. Hoffman, "Design and analysis of a wearable robotic forearm," in *Proc. IEEE Int. Conf. Robot. Automat.*, 2018, pp. 5489–5496.
- [6] K. R. Saul et al., "Benchmarking of dynamic simulation predictions in two software platforms using an upper limb musculoskeletal model," Comput. Methods Biomech. Biomed. Eng., vol. 18, no. 13, pp. 1445–1458, 2015.
- [7] P. H. Nguyen, C. Sparks, S. G. Nuthi, N. M. Vale, and P. Polygerinos, "Soft poly-limbs: Toward a new paradigm of mobile manipulation for daily living tasks," *Soft Robot.*, vol. 6, no. 1, pp. 38–53, 2019.
- [8] M. Rossero, A. S. Ciullo, G. Grioli, M. G. Catalano, and A. Bicchi, "Analysis of compensatory movements using a supernumerary robotic hand for upper limb assistance," *Front. Robot. AI*, vol. 7, p. 200, 2020.
- [9] S. L. Delp et al., "OpenSim: Open-source software to create and analyze dynamic simulations of movement," *IEEE Trans. Biomed. Eng.*, vol. 54, no. 11, pp. 1940–1950, Oct. 2007.
- [10] L.-F. Lee and B. R. Umberger, "Generating optimal control simulations of musculoskeletal movement using OpenSim and MATLAB," *PeerJ*, vol. 4, 2016, Art. no. e1638.
- [11] B. J. de Kruif, E. Schmidhauser, K. S. Stadler, and L. W. O'Sullivan, "Simulation architecture for modelling interaction between user and elbow-articulated exoskeleton," *J. Bionic Eng.*, vol. 14, no. 4, pp. 706–715, 2017.
- [12] P. Agarwal, P.-H. Kuo, R. R. Neptune, and A. D. Deshpande, "A novel framework for virtual prototyping of rehabilitation exoskeletons," in *Proc. IEEE Int. Conf. Rehabil. Robot.*, 2013, pp. 1–6.
- [13] S. M. LaValle, *Planning Algorithms*, Cambridge, UK: Cambridge University Press, 2006.
- [14] M. Kalakrishnan, S. Chitta, E. Theodorou, P. Pastor, and S. Schaal, "STOMP: Stochastic trajectory optimization for motion planning," in *Proc. IEEE Int. Conf. Robot. Automat.*, 2011, pp. 4569–4574.
- [15] L. U. Odhner, R. R. Ma, and A. M. Dollar, "Open-loop precision grasping with underactuated hands inspired by a human manipulation strategy," *IEEE Trans. Autom. Sci. Eng.*, vol. 10, no. 3, pp. 625–633, Jul. 2013.
- [16] J. Y. Luh, M. W. Walker, and R. P. Paul, "On-line computational scheme for mechanical manipulators," *J. Dyn. Syst., Meas., Control*, vol. 102, no. 2, pp. 69–76, 1980.
- [17] A. V. Hill, "The heat of shortening and the dynamic constants of muscle," *Proc. Royal Soc. London. Series B-Biol. Sci.*, vol. 126, no. 843, pp. 136–195, 1938.
- [18] L. M. Schutte, M. M. Rodgers, F. Zajac, and R. M. Glaser, "Improving the efficacy of electrical stimulation-induced leg cycle ergometry: An analysis based on a dynamic musculoskeletal model," *IEEE Trans. Rehabil. Eng.*, vol. 1, no. 2, pp. 109–125, Jun. 1993.
- [19] D. G. Thelen, F. C. Anderson, and S. L. Delp, "Generating dynamic simulations of movement using computed muscle control," *J. Biomech.*, vol. 36, no. 3, pp. 321–328, 2003.
- [20] R. H. Byrd, M. E. Hribar, and J. Nocedal, "An interior point algorithm for large-scale nonlinear programming," SIAM J. Optim., vol. 9, no. 4, pp. 877–900, 1999.
- [21] G. M. Gasparri et al., "Efficient walking gait generation via principal component representation of optimal trajectories: Application to a planar biped robot with elastic joints," *IEEE Robot. Automat. Lett.*, vol. 3, no. 3, pp. 2299–2306, Jul. 2018.